Proceedings of the 2000 IEEE
International Conference on Robotics & Automation
San Francisco, CA • April 2000

Constrained Force Control of Shape Memory Alloy Actuators

Danny Grant Vincent Hayward

Department of Electrical Engineering and
Research Centre for Intelligent Machines
McGill University
Montréal, Québec, H3A 2A7, Canada
grant@cim.mcgill.ca, hayward@cim.mcgill.ca

Abstract

Experimental results are presented to show that SMA actuators are able to control forces both rapidly and precisely. An antagonistic pair of constrained actuators is shown to be capable of rapidly changing the setpoint throughout a ± 7.00 N range. Although the system entered into a limit cycle at the setpoint, the limit cycle magnitude was small. The peak to peak amplitude of the limit cycles was only 0.07 N with a worst case average offset of 0.016 N at high force rates up to 75 N.s^{-1}. Simulation results also indicate that accuracy could be improved with an increased sampling rate. The SMA actuator pair was also shown to be capable of accurate tracking. The maximum tracking error for a f = 0.500 Hz, 2.00 N sine wave was 0.04 N. For the 2.00 Hz tracking, the maximum error was approximately equal to the boundary layer width which was set at 0.30 N.

1 Introduction

There are a number of applications that require a force to be applied without significant motion, such as in the case of a robot gripper. SMA's are well suited for force control applications due to their high strength to weight ratio. The force control of a pair of constrained SMA actuators will be examined in this paper to demonstrate the high force capabilities of the SMA actuator first presented in [3].

2 Modelling

A vast amount of research has been undertaken in modelling SMA's, particularly in capturing their hysteresis properties. Models range from considerations of the atomic interactions of the separate alloys, as by Kafka [5], to experimentally fitting nonlinear differential equations to the input-output relations, as by Arai et. al. [1].

Some of the earlier models that were employed for control purposes are: Kuribayashi's model [6] based on experimentally identified relations, the sub-layer model of Ikuta [4], and the constitutive equation of Tanaka [8]. Shahin et. al. [7] explored the heat transfer relations for SMA fibers considering three cases for cooling: that of free convection, forced convection and employing the Peltier effect.

A model was proposed in [2] to give the following force current relationship for a single SMA actuator:

$$F = \frac{a_f n}{K_g} K_p \left[\int_o^{t_f} I_f^2(t) R_f dt + C_i \right], \qquad (1)$$

where n is the number of fibers, K_g the displacement gain, a_f the fiber cross sectional area, I_f the current per fiber, R_f the fiber resistance, C_i is an integration constant and K_p is given by:

$$K_p = \frac{(\Theta - K_m \Omega)}{m_f (c_p (1 - K_m c_m \Omega) + \Delta h K_m (1 - c_m \Theta))}. \qquad (2)$$

where c_p is the specific heat, Δh the latent heat, $\frac{1}{c_m}$ the stress rate, A_{so} the austenite start temperature, A_{fo} the austenite finish temperature, K_m a material constant, Θ a thermoelastic constant, Ω a transformation constant and m the mass of the fiber.

Equation 1 results in an explicit input-output relationship for the heating of a single SMA fiber which provides the key to determining the force model for the SMA actuator.

Theoretical modelling and open loop experiments have shown that the antagonistic force response of the SMA actuator behaves like an integrator while the input current is applied. When there is zero input, the system behaves like a first order system, slowly resetting back to the neutral position. This behaviour can

be modelled by a 'leaky' integrator, which is in essence a first order system. The antagonistic system however has two inputs, one for each actuator. One of the constraints of this antagonistic arrangement is that at no time should both actuators be driving the system, as this will cause excessive stress on the alloy and damage the shape memory effect. The two actuator inputs then can be considered as a single signal, the positive portion corresponding to one actuator and the negative portion to the other. A block diagram of the open loop model for the antagonistic force system is given in Figure 1.

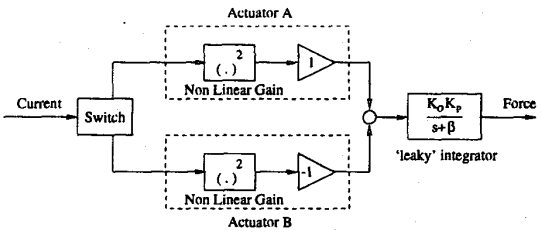

Figure 1: Open loop force model

The 'switch' block routes the input to the active actuator A or B, whether the input is positive or negative, and routes zero to the passive actuator. The negative gain is needed as the nonlinear gain will be an even power of the current magnitude.

2.1 Force Test Bed

For the constrained force experiments, two antagonistic SMA actuators were arranged as shown in Figure 2. The actuators are coupled to the test bed and to a rigid beam connected to the force sensor by threaded rods. Note that each actuator consists of 12 fibers in parallel.

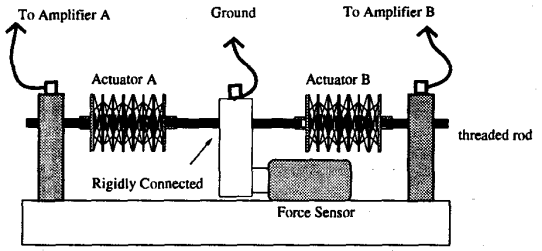

Figure 2: Force test bed

The force setup employed an ultra-precision mini load-cell from Transducer Techniques^{TM} (MDB-2.5) connected through a rigid beam to the SMA actuators. This allowed measurement up to 10 N with a precision of $\pm$ 0.01 N.

3 Control

To compensate for the difficulties in realizing practical SMA devices, relay control will be employed. Relay control has a number of advantages when applied to the control of SMA's, including robustness to parametric uncertainty and ease of implementation, both computationally and physically. One of the most important advantages of using relay control is that it circumvents the input-output hysteresis that makes SMA's difficult to control [2].

A two stage multi-relay was initially explored for the control of the SMA actuator for position in [3]. This same controller can be used to control the force. For this controller, two constant amplitude current values are used depending on the magnitude of the error. When the error is large, a high value of current is used to drive the plant quickly to the setpoint which will be referred to as I_H. As the error approaches zero, a lower magnitude pulse, I_L, is used to minimise the limit cycle magnitude. This results in a smoother motion as the state trajectory slows down when it approaches the setpoint switching surface, allowing the dual requirements of stability and a quick response to be satisfied. A block diagram of the controller is shown in Figure 3.

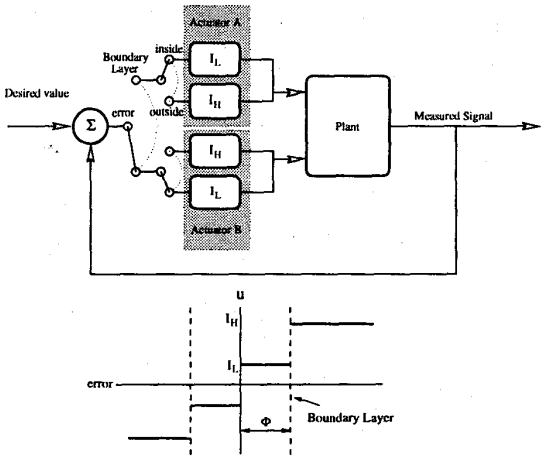

Figure 3: Two stage controller

The design variables in the controller are the mag-

nitudes of the constant current pulses, I_H and I_L, and the width of the boundary layer, ϕ, around the switching surface as shown at the bottom of Figure 3. Positive values of the feedback correspond to one actuator and negative values to the other. The magnitude of the I_H pulse is directly proportional to the speed of response. The magnitude of the I_L pulse needs to be chosen high enough to maintain the temperature of the actuator at the setpoint, that is, a current that will provide enough heat to compensate for the ambient heat loss.

4 Results

4.1 Simulated Force Response

The first order model of the force current relation is determined by the overall gain $K_O K_p$, and the location of the pole, β. These two parameters were adjusted to account for the closed loop observed performance as is detailed in [2]. After setting these parameters it is possible to modulate I_H, I_L and ϕ in the controller and obtain a good match between the simulated and experimental results.

4.1.1 Step Response

The simulated response to a series of desired force steps from 1.0 N to 7.0 N in $Simulink^{TM}$ is shown in Figure 4 where the desired response is represented by a dashed line and the simulated response by a solid line. The model parameters are set to $K_p = 2.50$ and $\beta = 0.90$, with the two stage controller values set to $I_H = 0.375$ A, $I_L = 0.175$ A, and $\phi = 0.30$ N. A sample and hold block was implemented in the simulation with the hold set equal to the experimental sampling frequency (1 KHz) to observe the effects of the finite sampling.

Figure 4(a) shows the complete output response from $t = 0$ ms to $t = 4000$ ms. Figure 4(b) shows a close up of the section where the desired step is applied from $t = 450$ ms to $t = 650$ ms. The steady state response of the desired inputs 2.0 N and 7.0 N are shown in Figure 4(c) and (d) respectively.

Examining Figure 4(b) it can be seen that the response of the actuator system resembles that of an ideal integrator. The rise time is proportional to the desired input magnitude, and the speed of response to the magnitude of the current pulse. Although the model is first order, the output response resembles an integrator since the slow pole, β does not have a significant effect when the I_H pulse is active. The effect

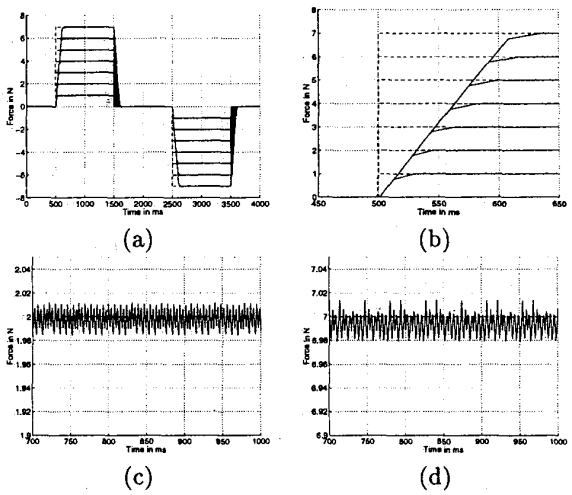

Figure 4: Closed loop force simulation response for a constrained pair of antagonist SMA actuators: Dashed line = desired response; Solid line = simulated response (a) Series of steps (b) Detailed series of steps (c) Steady state $F_d = 2.0$ N and (d) Steady state $F_d = 7.0$ N.

of the pole is more pronounced inside the boundary layer, when the I_L pulse is active. The slope of the response inside the boundary layer can be seen to decrease as the magnitude of the desired input increases, as can be seen in Figure 4(b). This is a result of the pole β having more of a 'leak' effect on the system output as the system response moves from the neutral point.

The transition from the I_H to I_L pulse can be seen when the trajectory enters the boundary layer around the setpoint, and the slope of the output response changes, for example at $t = 575$ ms for the 5.0 N desired step in Figure 4(b). The decrease in the speed of response results in a performance penalty in the time domain, but is necessary to keep the limit cycle magnitude low.

As the force model is first order, the simulated system does not contain an inertial term. The apparent limit cycles in the steady state responses of Figures 4(c) and (d) are caused by the sample and hold block of the simulation. Sampling at a higher frequency would attenuate this effect. The magnitude of the limit cycle caused by this finite sampling will give a benchmark to compare with the experimentally observed limit cycles.

4.1.2 Tracking

Having examined the simulated closed loop step response, the simulated tracking response will now be examined. The modelled response to a variety of sine waves of differing magnitude and frequency can be seen in Figure 5 where the dashed line represents the desired response and the solid line the simulated response. Figure 5(a) is the simulated response to a 2.0 N amplitude sine wave of 0.5 Hz. The magnitude is increased to 6.0 N for Figure 5(b). Figure 5(c) is the response to a 2.0 N sine wave of 1.0 Hz , and the frequency is increase to 2.0 Hz for Figure 5(d).

The response tracks the 2.0 N sine wave of 0.5 Hz of Figure 5(a) almost perfectly, but the 6.0 N amplitude response of the same frequency in Figure 5(b) begins to lag behind. This is a result of the modelled actuator pair being able to achieve a finite rate, limited by the I_L pulse magnitude. This limit on the rate results in a limit on the slope of the desired response the system can accurately track. As the input frequency increases, the system lags further behind the desired response as shown in Figure 5(d). The amount of lag here is equal to the boundary width ϕ as the system oscillates between the I_H and I_L pulses along the boundary layer threshold.

Due to the finite sampling rate, the simulated response oscillates around the desired waveform as shown in Figure 5(e) and (f). When the desired velocity is high, the simulated system is always catching up to the desired waveform as shown in Figure 5(e). At the peaks of the sine waves the simulation oscillates around the desired signal. As the frequency increases the simulation lags behind the desired waveform by an amount equal to the boundary layer width, as shown in Figure 5(g) where the force response is always 0.30 N behind the desired response. Here the controller is alternating between the I_H and I_L magnitude pulses, causing the system to ride along the boundary layer. At the peaks of the 2.0 Hz wave, the simulated system catches up to the desired waveform and again oscillates around the setpoint for a short time.

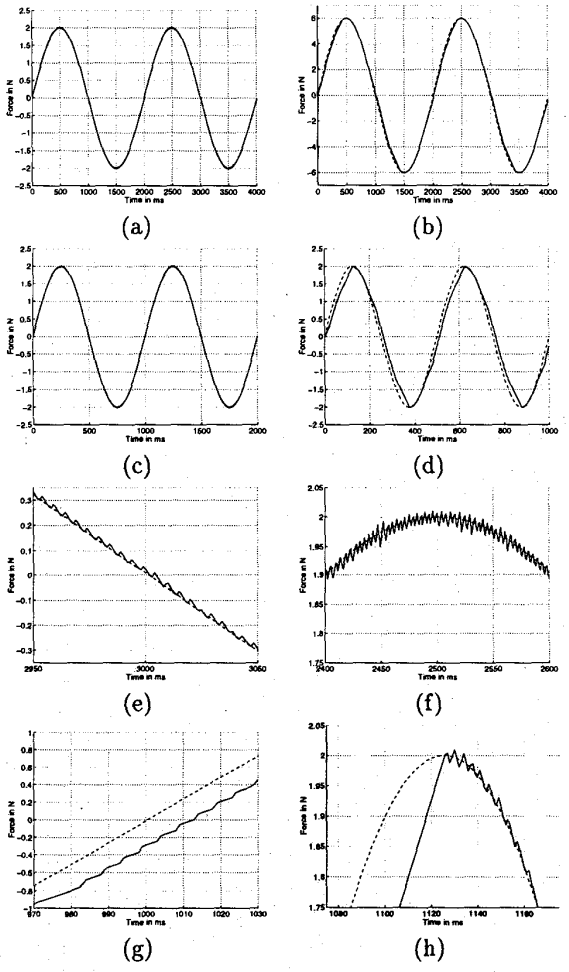

Figure 5: Closed loop force simulation tracking ($A\sin(2\pi ft)$): Solid line = simulated; Dashed line = desired (a) A = 2.0 N, f = 0.5 Hz (b) A = 6.0 N, f = 0.50 Hz, (c) A= 2.0 N, f = 1.0 Hz, (d) A = 2.0 N, f = 2.0 Hz, (e),(f) detailed A = 2.0 N, f = 0.5 Hz, and (g)(h)detailed A = 2.0 N, f = 2.0 Hz.

4.2 Experimental Force Response

The experimental step response and tracking will now be examined and compared with the simulation results of the previous section. Using the experimental testbed of Figure 2, the two stage controller was applied to the actual system. The noise level of the load cell was ± 0.009 N. A dead band was placed around the force setpoint with magnitude ± 0.01 N for the experimental implementation to avoid spurious switching on

the noise. The controller gains were set identically to: $I_H = 0.375$ A, $I_L = 0.175$ A, and $\phi = 0.30$ N.

4.2.1 Step Response

The experimental response to a similar series of desired input steps of the simulations in Figure 4 can be seen in Figures 6(a) and (b). Figures 6(c) and (d) show the detailed steady state response for desired force steps of 2.0 N and 7.0 N respectively.

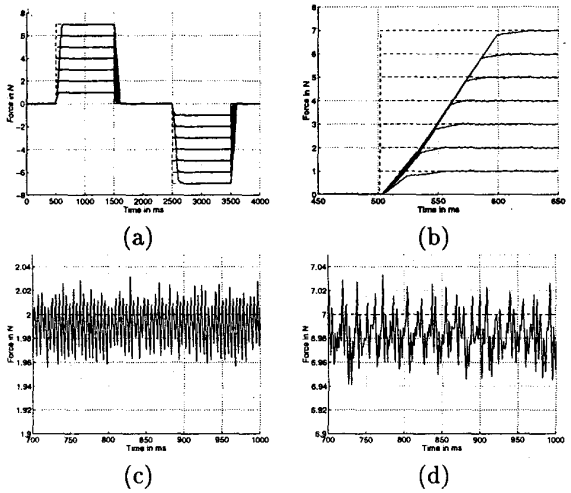

Figure 6: Closed loop force experimental response for a constrained pair of antagonist SMA actuators: Solid line = experimental; Dashed line = desired (a) Series of steps (b) Detailed series of steps (c) Limit cycle for Fd = 2.0 N and (d) Limit cycle for Fd = 7.0 N. The corresponding simulations are in Figure 4

Examining Figure 6(b) it can be seen that the experimental response of the actuator system resembles that of the simulated response and is similar to the response of an integrator. The responses of the 1.0 N and 2.0 N magnitude desired steps are notably different from the others. For the experimental results in Figure 6 two smaller magnitude desired pulses were applied before time = 0 so that the actuators would not start out completely 'cold', however for the smaller desired pulses the effects of starting 'cold' can still be seen.

Due to the switching nature of the controller and the finite sampling rate, the system enters a low magnitude limit cycle at the setpoint, as shown in Figures 6(c) and (d). This limit cycle is fairly regular at 2.0 N but increases in irregularity as the limits of the device are approached for the desired 7.0 N step. A multi-periodic limit cycle is shown in Figure 6(d). The multi-periodic limit cycle roughly consists of two frequencies as the system falls below the setpoint and then exhibits several oscillations before intersecting the setpoint again.

Table 1 summarises the quantitative limit cycle properties for the simulated and experimental trials for the 2.0 N and 7.0 N cases.

Setpoint in N	Peak to Peak in N		Average Offset in N		Frequency in Hz	
	Sim	Exp	Sim	Exp	Sim	Exp
0.0	.002	.07	.0000	.005	250	217
2.0	.003	.07	.002	.008	250	215
7.0	.003	.07	.007	.016	250	X

Table 1: Table of limit cycle parameters

From Table 1 the peak to peak amplitude of the limit cycles is only 0.07 N with the maximum average offset of 0.016 N. Considering that the range of force outputs is ± 7 N this results in a resolution measure of 0.50%. This accuracy is obtained with high force rates up to 75 $N.s^{-1}$.

Comparing the peak to peak magnitudes of the simulated and experimental limit cycles, indicates that the finite sampling rate accounts for almost half of the peak to peak magnitude of the limit cycle. This indicates that the limit cycle could be even further reduced by using a higher sampling rate.

4.2.2 Tracking

Force tracking experiments similar to the simulations of Figure 5 were also conducted on the actual system using a variety of sine wave desired inputs as shown in Figure 7. In the initial part of the curve of Figure 7(a), the tracking is poor as the actuator pair heats up. After approximately 1.5 s the system tracking is accurate. For the larger magnitude sine wave of Figure 7(b) the experimental response can be seen to lag behind the system. Similarly, as we increase the frequency of the input in Figures 7(c) and (d) the response lags behind the input due to the finite rate of the actuator pair.

In Figure 7(e) in can be seen that the experimental response is always catching up to the desired waveform, and in Figure 7(f) it oscillates around the dead band layer (0.01 N before the setpoint) when the tracking rate is low. As the frequency increases, the experimental response lags behind the desired waveform by the boundary layer width, as shown in Figure 5(g),

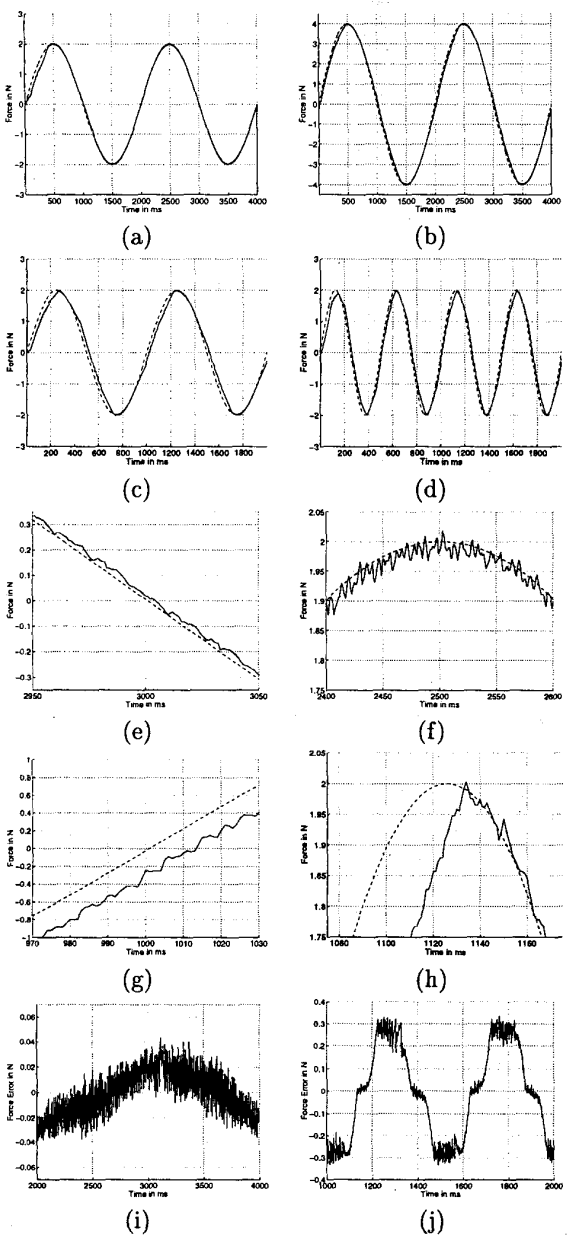

Figure 7: Closed loop force experimental tracking ($A\sin(2\pi ft)$): Solid line = experimental; Dashed line = desired (a) A = 2.0 N, f = 0.5 Hz, (b) A = 4.0 N, f = 0.5 Hz, (c) A= 2.0 N, f = 1.0 Hz (d) A = 2.0 N, f = 2.0 Hz (e)(f) detailed A = 2.0 N, f = 0.5 Hz, (g)(h) detailed A= 2.0 N, f = 2.0 Hz, (i) tracking error A = 2.0 N, f = 0.5 Hz, and (j) tracking error A = 2.0 N, f = 2.0 Hz. The corresponding simulations are in Figure 5

and catches up to the desired response at the peaks, as in Figure 5(h).

The tracking error for the $f = 0.5$ Hz sine wave and $f = 2.0$ Hz sine wave are shown in Figures 7 (i) and (j). Note that the initial errors due to the actuators starting 'cold' are not shown. The maximum tracking error for the 0.5 Hz sine wave is 0.04 N, and this occurs when the sine wave is at its peak velocity at the zero position. The range of the requested sine wave is ± 2.0 N so this corresponds to a resolution measure of 1.0%.

For the 2.0 Hz tracking, the maximum error is approximately equal to the boundary layer width as can be seen in Figure 7(f), resulting in a resolution measure of 7.5%. Although not experimentally tested, this level of accuracy with the 2.0 N sine wave should hold for frequencies up to 6 Hz as the force rate of the I_H pulse is approximately 75 N.s^{-1}.

4.3 Continuous Operation

During continuous operation the average 'cold' temperature will increase. To investigate this effect, the force controller was applied to the testbed of Figure 2 for a repeated waveform. The repeated waveform consisted of a step of 4.0 N in the positive direction and then a 4.0 N step in the negative direction as shown in Figure 8(a).

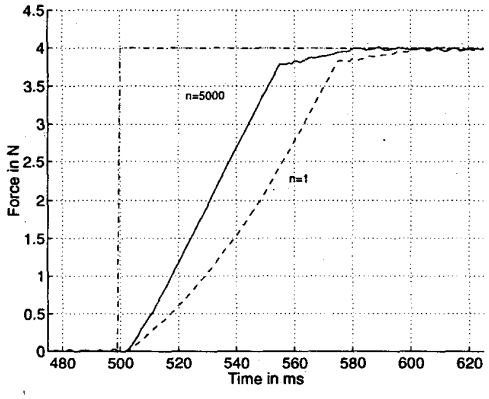

Figure 8: Continual operation force response Dashed line = first iteration; Solid line = 5000 iteration

The response to the positive 4.0 N step for the first iteration and the 5000th iteration is shown in Figures 8. Operating for 5000 cycles corresponded to a continuous operation for approximately 5.5 hours.

Although the thermal steady state performance is indicated by the 5000th iteration, this performance is actually reached after only a few = cycles. Figure 8 indicates that during continuous operation the temperature setpoint increases. This has the effect of reducing the nonlinear section of the initial heating curve. It also results in an increased gain with an associated faster rate of response. The linearisation effect of the continuous operation is apparent when the I_H pulse is active where the force rate for the 5000th iteration is basically constant at 75 $N.s^{-1}$.

5 Summary

The experimental results indicate that the SMA actuators are able to control forces both rapidly and precisely. The system was shown to be capable of rapidly changing the setpoint throughout a ± 7.00 N range. Considering that a single actuator weighs approximately 6 g, and most of this weight could be shed by redesigning the actuator brass end disks, this results in a high strength to weight ratio. Although the system entered into a limit cycle at the setpoint, the limit cycle magnitude was small. The peak to peak amplitude of the limit cycles was only 0.07 N with a worst case average offset of 0.016 N. This corresponds to an accuracy measure of 0.50%, which was obtained with high force rates up to 75 $N.s^{-1}$. The simulation results also indicate that accuracy could be improved with an increased sampling rate.

The SMA actuator pair was also shown to be capable of accurate tracking. The maximum tracking error for a $f = 0.500$ Hz, 2.00 N sine wave was 0.04 N. For the 2.00 Hz tracking, the maximum error was approximately equal to the boundary layer width which was set at 0.30 N. Due to the high force rate generated by the I_H pulse this level of accuracy should be maintained to frequencies up to 6 Hz.

Continuous operation experiments verified that the average 'cold' temperature of the alloy will increase with continual operation. This has the beneficial effects of increasing the rate of response and linearising the system. The linearised experimental response also matches well with the proposed force model, therefore justifying the numerous reductions made in the modelling process.

Acknowledgements The research was mostly funded by IRIS (Phase II), the Institute for Robotics and Intelligent Systems part of Canada's National Centres of Excellence program (NCE), under the heading "Machine Sensing and Actuation: Computational Sensing for Vision and Robotics" (MSA-4), and an operating grant from NSERC, the National Science and Engineering Council of Canada.

References

[1] K. Arai, S. Aramaki, and K. Yanagisawa. Continuous system modelling of shape memory alloy (sma) for control analysis. In *1994 5th International Symposium on Micro Machine and Human Science Proceedings*, pages 97–99, Nagoya, Japan, October 1994. IEEE.

[2] D. Grant. *Accurate and Rapid Control of Shape Memory Alloy Actuators.* PhD thesis, McGill University, 1999.

[3] D. Grant and V. Hayward. Design of shape memory alloy actuator with high strain and variable structure control. In *Proceedings of 1995 IEEE International Conference on Robotics and Automation*, volume 3, pages 2305–2312, Nagoya,Aichi,Japan, May 21-27 1995.

[4] K. Ikuta, M. Tsukamoto, and S. Hirose. Mathematical model and experimental verification of shape memory alloy for designing micro actuator. In *Proc. of the IEEE MicroElectroMechanical Systems Conference*, pages 103–108, 1991.

[5] V Kafka. Shape memory: A new concept of explanation and of mathematical modelling. part i: Micromechanical explanation of the causality in the sm processes. *Journal of Intelligent Material Systems and Structures*, 5(6):809–814, November 1994.

[6] K. Kuribayashi. A new actuator of a joint mechanism using TiNi alloy wire. *The Int. Journal of Robotics Research*, 4(4), 1986.

[7] Ali R Shahin, Peter H Meckl, James D Jones, and Mark A Thrasher. Enhanced cooling of shape memory alloy wires using semiconductor "heat pump" modules. *Journal of Intelligent Material Systems and Structures*, 5(1):95–104, 1994.

[8] Y. Tanaka. A thermomechanical sketch of shape memory effect: One-dimensional tensile behavior. *Res Mechanica, the International journal of Structural Mechanics and Materials Science*, 18(1):251–63, 1986.